Applied Mathematics & Information Sciences
An International Journal

http://dx.doi.org/10.18576/amis/180519

The Influence of Thickness and Mesh Orientation on The Impact Resistance Performance of Geogrid Reinforced Oil Palm Shell Concrete

Zakaria Che Muda[1,], Mohamed Hafez[1], Md. Asraful Alam[2], Ghazal Malik[3], and As'ad Zakaria[4]*

[1]Faculty of Engineering and Quantity Surveying, INTI-International University, Nilai, Malaysia
[2]Department of Civil Engineering, University of Asia Pacific, Level-6, 74/A, Green Road, Farmgate, Dhaka-1215, Bangladesh
[3]Department of Civil Engineering, Nasional Energy University, Putrajaya Campus, Jalan Kajang - Puchong, 43000 Kajang, Malaysia
[4]Institute of Energy Systems, School of Engineering, University of Edinburgh, Edinburgh EH9 3FB, UK

Received: 1 Mar. 2024, Revised: 15 Apr. 2024, Accepted: 2 May 2024.
Published online: 1 Sep. 2024

Abstract: The utilization of agricultural waste recycling, using oil palm shell lightweight aggregate in concrete, has been developed as a green product for the construction industry. This innovation aims to mitigate environmental pollution and promote sustainable practices in industrial waste management. This research paper investigates the effect of thickness and geogrid orientation on the impact performance of lightweight oil palm shell concrete slab reinforced with geogrid under low-velocity impact projectile. Slabs of dimensions 300mm x 300mm and 40mm thickness are subjected to a drop-weight impact test using a self-fabricated rig and a 1.25 kg steel ball dropped from a height of 1.0 m. The study's main objectives are to analyze the relationship between impact energy, crack resistance, crack resistance ratio, and impact residual strength ratio against the thickness and the geogrid orientations for various OPS mix variants. The highest impact performance is the 0.45OPS variant with geogrid followed by 0.50OPS and then 0.60OPS. The results indicate that an increase in thickness leads to significant improvements; however, the change in geogrid orientation from the cross direction (CD) to the main direction (MD) had a slight improvement in the impact behavior of the slab. The linear and bi-linear equations were proposed for different under-service and ultimate impact behavior against thickness for various OPS mix variants without and with geogrid. The ultimate condition has a higher number of segmental failure zones as compared with the service condition. The geogrid mesh bridges the micro-cracks at service conditions and major cracks at the failure phase, preventing the slab from totally collapsing.

Keywords: waste recycling, green products, oil palm shell aggregate, impact behavior, geogrid, support boundary conditions.

1 Introduction

Using agricultural waste recycling, an oil palm shell lightweight aggregate concrete (LWAC) has been developed as a green product for the construction industry. This eco-friendly approach seeks to address environmental pollution and promote sustainable practices in industrial waste management. The quest for sustainable agriculture waste as a green product has recently been reviewed by many researchers (Nadeem et al., 2020; Raut& Ghosh, 2020; Kumar & Bhunia,2021; Sharifi et al., 2021; Mukherjee et al., 2021; Naik et al., 2021). Alsayed and Alsayed (2019) examine the advantages and challenges of using agricultural waste in construction materials, including sustainability, environmental impact, technical performance, and economic feasibility. It discussed the potential benefits of using agricultural waste materials in terms of reducing the consumption of traditional resources, promoting waste management, and minimizing construction's carbon footprint. Agricultural waste aggregates, fibers, and ash derived from byproducts and residues have shown promise as replacements for traditional aggregates in concrete (Ganesh & Bhattacharyya, 2020; Anandan et al., 2017; Beddoe & Pearce, 2017). The study conducted by Farahani et al. (2017) provided evidence of the successful production of lightweight aggregate concrete by incorporating a high volume of agricultural and industrial waste materials. The research showcased the feasibility of creating lightweight aggregate concrete using these waste materials, thus highlighting its potential as a sustainable construction material.

Oil palm shell (OPS), a byproduct of the palm oil industry, can serve as structural lightweight aggregates in concrete, offering advantages such as good mechanical strength, low density, and thermal insulation properties. These materials provide a sustainable and eco-friendly solution for reducing the environmental impact of concrete production. It is

*Corresponding author e-mail: zakaria.chemuda@newinti.edu.my

crucial to study the impact strength characteristics and evaluate the performance of these materials for use in the building industry. Habeeb et al. (2016), Arunachalam & Umarani (2017), and Kareem et al. (2022) conducted a review that concluded using OPS as an alternative aggregate is effective and sustainable, based on positive results from previous studies. Aslam et al. (2015) investigated the production of structural lightweight aggregate concrete using locally available solid waste materials, namely oil palm shells and boiler clinkers as coarse lightweight aggregates. Okafor & Zain (2018) review the utilization of oil palm shells as a lightweight aggregate in concrete and examine its potential substitute for conventional lightweight aggregates in concrete production. The researchers evaluated its suitability and compatibility within concrete mixtures, exploring its performance and potential benefits. A study conducted by Abdul Rahman et al. (2020) researched the substitution of 80% of normal weight aggregate with lightweight oil palm shell (OPS) aggregate. The study showed a 16% reduction in density and a notable decrease of 35% in compressive strength compared to the control normal concrete.

Recent research studies have demonstrated the potential for achieving higher strength grades in OPS concrete. Mannan et al. (2006) achieved a compressive strength of 32.84 N/mm² by incorporating 20% polyvinyl alcohol in OPS concrete. Mo et al. (2014) obtained 28-day compressive strengths ranging from 37 to 49.4 MPa for OPS concrete, both with and without fibers. Maghfouri et al. (2018) observed a compressive strength of 40.5 N/mm² when using 100% OPS aggregate replacement. Aslam et al. (2017) found that incorporating 50% oil palm boiler clinker in OPS concrete resulted in a compressive strength of 53.3 N/mm².

The flexural load carrying capacity, deflection, and energy absorption of the geogrid reinforced slab, as compared to the steel-reinforced slab, increased by 25, 6.5, and 23%, respectively (Rajesh Kumar et al., 2022)

The combined geogrid and steel reinforcement embedded RC slab specimens sustained higher counts of impact loading blows, influencing the enhanced impact performance in terms of impact energy absorption and impact ductility index. The results showed that the RC slab combined with a geogrid reinforcement layer at both faces of the slab and the conventional steel reinforcement resisted concrete crushing by spreading the impact stress to a larger area (Vijay et al., 2020).

Similar studies to enhance the impact resistance of a slab using a geogrid reinforcement have been investigated by Mansouri et al. (2017), Han et al. (2018), Kheyroddin & Bocciarelli (2019), Wang et al. (2019), Niu et al. (2020) and Shi et al. (2021).

Impact resistance is a critical property that determines the ability of concrete to withstand repeated impacts and absorb energy without developing cracks or spalling. Two categories of impacts include low-velocity and high-velocity impacts. Mahmoud and Afroughsabet (2010) noted that the drop weight impact test, recommended by the ACI Committee 544 (1996), is the simplest testing method available. However, this test's limitations include its small sample size and test setup, which may not be suitable for assessing non-homogeneous concrete composites, non-uniform fiber distribution, reinforcement with mesh, or different boundary conditions.

Impacts can cause cracking on the distal face of the concrete due to the propagation of reflected tensile waves from the point of impact. In highly reinforced slabs, even though they possess high energy resistance, failure can still happen due to punching shear. Localized damage is observed at the point of contact during an impact event, which can be attributed to compression failure near the impact point (Yahaghi et al., 2016).

The impact resistance of lightweight concrete can be improved by including OPS, as indicated by the findings of various researchers (Md Din et al., 2017; Mohd Nawi et al., 2019; Nuruddin et al., 2011). Similar studies have also explored the impact resistance of lightweight concrete incorporating OPS as coarse aggregates and utilizing fiber reinforcement. These studies consistently demonstrate that adding fibers enhances the impact resistance of lightweight concrete containing oil palm shells (Md Akhir et al., 2020; Tahir et al., 2019; Liew et al., 2021; Yew et al., 2018). Che Muda et al. (2015) specifically investigated the performance of lightweight concrete slabs made with OPS and reinforced with geogrid under different support boundary conditions. Low-impact projectile tests were conducted, and it was observed that the presence of geogrid reinforcement led to increased first and ultimate crack resistance. The 4-support boundary condition showed improvements of up to 29.8% and 40.6% in first and ultimate crack resistance, respectively, compared to the 2-support condition. Anil et al. (2015) studied the support type and support layout of a bottom steel mesh reinforced with a 4mm diameter bar at 50mm spacing under a low-velocity impact loading. The number of blows for fixed supports is higher than those with hinge ones. In addition, the highest number of drops is obtained from the specimens supported on four sides, while the lowest number is obtained from the specimens supported on two adjacent sides.

Research on the impact resistance performance of lightweight OPS concrete reinforced with geogrid and considering different slab thicknesses and geogrid reinforcement orientations for various OPS contents and compressive strengths is currently limited in the existing research literature. Therefore, the primary objective of this paper is to investigate the influence of thickness and geogrid reinforcement direction on the impact performance for various OPS contents. Consequently, there is a need for further studies to explore the relationship between impact behavior against the thickness and geogrid orientation and

investigate its failure modes.

2 Materials

Oil palm shells (OPS), as depicted in Figure 1, possess distinctive physical properties that make them well-suited for replacing conventional aggregates. OPS are naturally sized, exhibiting hardness while being lighter in weight compared to traditional aggregates. This inherent lightness of oil palm shells renders them a suitable alternative for producing lightweight concrete. For this study, the OPS underwent sieving to achieve a specific size range between 8mm to 10mm.

In the mix design of OPS lightweight concrete using different OPS to cement ratio of 0.45, 0.5 and 0.6 were employed. The compressive strength values corresponding to each OPS content with its slump values are presented in Table 1. For all experimental concrete designs, Ordinary Portland Cement complying with ASTM Type I specifications was utilized, with a consistent water-cement ratio of 0.45. Silica fume, supplied by EIKEM, was incorporated into the mix. The specific gravity of the silica fume is 2.2, and its particle size measures 0.15 µm.

Fig 1: OPS Lightweight Aggregates (8 – 10 mm Size)

A superplasticizer, specifically Sika Viscocrete-15RM, was added to the mix at a dosage of 2% by weight of the cement. The specific gravity of the superplasticizer used in this study is 1.12.

The 0.45OPS, 0.50OPS, and 0.60OPS mix had a slump value of 100, 85, and 75 mm, respectively, representing medium workability fresh concrete. The 0.45OPS, 0.50OPS, and 0.60OPS mix have a structural grade concrete of C20/25 with a compressive strength of 28.5MPa, 27.5MPa, and 26.0 MPa, respectively.

Figure 2 illustrates a Type A 160/50 having characteristic short-term tensile strength of 160kN/m in the main direction (MD) and 50kN/m in the cross direction (CD). The geogrid is assembled to form a directional structure that maximizes load-carrying efficiency. The strength and flexibility of geogrid made it an ideal replacement for conventional steel reinforcement. Each slab has one layer of reinforcement.

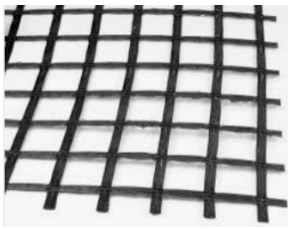

Fig. 2: Geogrid Reinforcement – Type A 160/50

3 Methodology

A risk matrix provides a valuable tool the likelihood of failure and the consequences arising from identified risk drivers associated with significant potential failure modes. In Figure 1, a dam risk matrix is depicted, employing general categories of failure likelihood and severity of the consequence.

3.1 Preparation of specimens

The configuration of a geogrid mesh with its orientation is shown in Figure 3. The slab configurations shown in Figure 3 are supported on two opposite edges with mesh main direction (MD) and cross direction (CD), as shown in Figure 3a. The slab has a control, as shown in Figure 3b, and geogrid mesh is placed at the bottom of the slab (Figure 3).

Table 1: Mixed Design and Compressive Strength

Mix Code (Fibre)	Binder		Aggregate		Water		SP		Slump	Compressive Strength
	Cement (kg)	Silica Fume (kg)	OPS (kg)	Sand (kg)	w/c	Wt (kg)	%	Wt (gm)	mm	MPa
0.45OPS	530	26.5	238.5	795	0.45	238.5	2	10.6	100	28.5
0.50OPS	530	26.5	265	795	0.45	238.5	2	10.6	85	27.5
0.60OPS	530	26.5	318	795	0.45	238.5	2	10.6	75	26.0

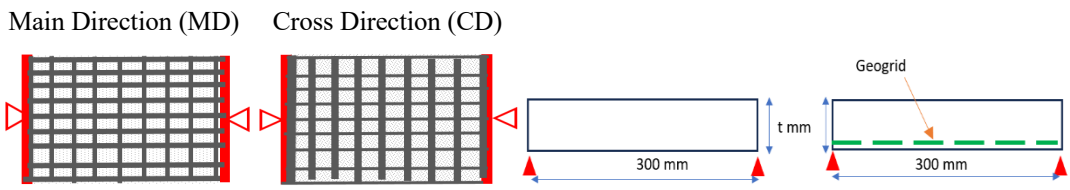

(a) Geogrid Orientation (b) Control (c) Geogrid Mesh at the bottom

Fig. 3: Slab Configuration

Table 2: Specification of Test Specimens

Mix Code	Compressive Strength, fcu (MPa)	Thickness (mm)	Direction of Geogrid	No of Slab Specimen Tested
0.45OPS Control	28.5	20	-	1
0.45OPS Control	28.5	30	-	1
0.45OPS Control	28.5	40	-	1
0.5OPS Control	27.5	20	-	1
0.5OPS Control	27.5	30	-	1
0.5OPS Control	27.5	40	-	1
0.6OPS Control	26.0	20	-	1
0.6OPS Control	26.0	30	-	1
0.6OPS Control	26.0	40	-	1
0.45OPS -MD	28.5	20	MD	1
0.45OPS- MD	28.5	30	MD	1
0.45OPS- MD	28.5	40	MD	1
0.45OPS -CD	28.5	20	CD	1
0.45OPS- CD	28.5	30	CD	1
0.45OPS- CD	28.5	40	CD	1
0.5OPS -MD	27.5	20	MD	1
0.5OPS- MD	27.5	30	MD	1
0.5OPS- MD	27.5	40	MD	1
0.5OPS -CD	27.5	20	CD	1
0.5OPS- CD	27.5	30	CD	1
0.5OPS- CD	27.5	40	CD	1
0.6OPS -MD	26.0	20	MD	1
0.6OPS- MD	26.0	30	MD	1
0.6OPS- MD	26.0	40	MD	1
0.6OPS -CD	26.0	20	CD	1
0.6OPS- CD	26.0	30	CD	1
0.6OPS- CD	26.0	40	CD	1

Table 2 contains the specification of the test specimens and the number of samples required for the experimental works. 27 sample slabs were cast and tested for the 0.45OPS, 0.5OPS, and 0.6OPS variants with control and geogrid orientations.

Before mixing, the OPS lightweight aggregates a pre-soaked in water for 24 hours, and the excess surface water is removed to achieve a saturated surface dry condition. The cement is placed in the mixer with the OPS aggregates and mixed for about 5 minutes. Later, the mixing water with SP is added to the mixture and mixed for another 5 min. The slabs are cast and compacted in the formwork as shown in Figure 4a and, demoulded after 24 hours and submerged in the water for 28 days curing. The surface is white washed with paint before testing as shown in Figure 4b.

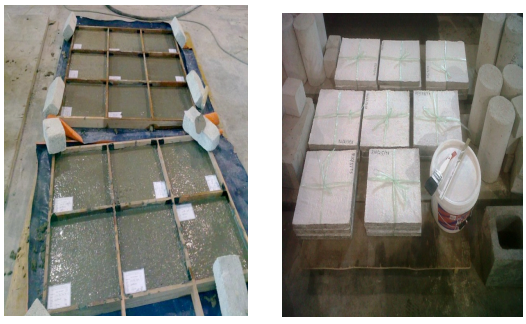

(a) Casting of slabs (b) Surface whitewash

Fig. 4: Preparation of the Slab Specimens

3.2 Test setup and testing of specimens

The study used a low-velocity drop-weight impact test using a steel ball weighing 1.25 kg with a drop height of 1.00 m impacting the specimen of size 300mm x 300mm with a variable thickness of 20, 30 and 40 mm mounted on the rectangular steel rack frame and supported on all its sides as shown in Figure 5.

Fig. 5: Impact Test Rig

At the service (first) crack and ultimate (failure) crack, the total crack length, the crack depth, the total number of blows recorded, and the crack width are measured by filler gauge as shown in Figure 6 with the total number of blows recorded.

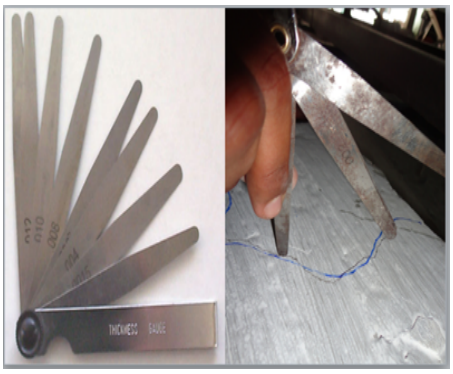

Fig. 6: Crack Width Measurement Feeler Gauge.

The slump test follows BS EN 12350-2:2009, and the compressive strength test is carried out on 100 mm cube specimens following BS EN 12390-4:2009.

3.3 Theory

The potential energy from the drop body is absorbed as strain energy, generating stresses that cause cracks in the target element. The width, depth, and length of the crack developed, and its failure mode are associated with the intensity of the energy, the amount of energy absorbed, and the properties of the concrete. It is assumed that the specimens fully absorb the total computed energy imparted.

The relationship between the potential energy of a drop-weight projectile and the strain energy dissipated in crack development is expressed as the following formula.

$$e = m \; x \; g \; x \; h \quad (1)$$

$$Es = Ns \; x \; e \quad (2)$$

$$Eu = Ns \; x \; e \quad (3)$$

where e = energy per blow (Joules), m = mass of steel ball (kg), g = 9.81 m/s^2, h = height of drop (m), Es = service impact energy (J), Eu = ultimate impact energy (J), Ns = No of blows at the first crack (service) and Nu = No of blows at failure (ultimate) crack.

Crack resistance was calculated using the following formulas, which were proposed by Kankam (1999);

$$Rs = Es / (l_c \; x \; d_c \; x \; w_c) \quad (4)$$

$$Ru = Eu / (l_c \; x \; d_c \; x \; w_c) \quad (5)$$

where Rs = Service crack resistance (N/mm^2), Ru = ultimate crack resistance(N/mm^2), l_c = total length of all cracks (mm), d_c = maximum crack depth (mm) and w_c = maximum crack width (mm).

Another dimensionless factor is a crack resistance ratio, which measures the ratio of ultimate crack resistance against the compressive strength of the concrete. It measures the effectiveness of the crack resistance performance against its compressive strength.

The crack resistance ratio was also defined by Equation 6 as;

$$Cr = Ru / f_{cu} \quad (6)$$

where Cr = Crack resistance ratio, Ru = ultimate crack resistance (N/mm^2), f_{cu} = cube compressive strength.

In order to easily evaluate quantitatively the improvement in the impact resistance characteristics, the impact residual strength ratio (I_{RS}) was formulated as the ratio of ultimate impact energy over service impact energy as given in Equation 7 (Ramakrishna and Sundararajan, 2005);

$$I_{RS} = Eu / Es \quad (7)$$

where I_{RS} = Impact strength ratio, Es = service impact energy (J), Eu = ultimate impact energy (J).

The impact residual strength ratio helped to evaluate the post-crack behaviour of the composites easily and could also be taken as a measure of the ductility imparted by the reinforcement incorporated into the slab.

4 Results and Discussion

The experimental impact test results are given in Appendix 1. These results are used to plot the impact behavior against the fiber VF and its fiber distributions.

4.1 Compressive Strength Relationship with OPS Content

Figure 7 indicates the relationship between compressive strength f_{cu} against the OPS content.

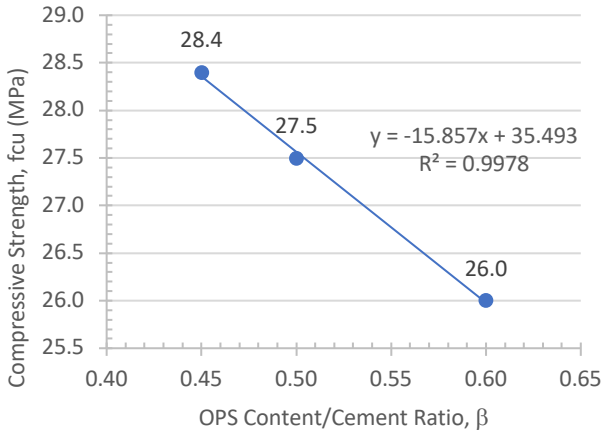

Fig. 7: Relationship between Compressive Strength, f_{cu} against OPS Content

As the OPS content increases, the 28-day compressive strength decreases with equation 8.

There is a good linear relation with an R^2 value of 0.9978 between the compressive strength and OPS Content as follows;

$$f_{cu} = -15.857b + 35.493 \quad (8)$$

where □ is the ratio of OPS/Cement by weight.

This indicates that the addition of OPS at higher content harms compressive strength. In

LWAC, the weakest path of the breakage is through the aggregates. The higher the content of the aggregates, the lower the load transfer efficiency and, thus the reduction in the compressive strength.

4.2 Impact Energy

Figure 8 depicts the 3-D histogram plot between the service and ultimate impact energy against the thickness.

The service and ultimate impact energy absorption of slab specimen increased with increased in thickness and compressive strength. By orientation of the mesh, the main direction is only marginally effective than the cross direction for the service and ultimate impact energy absorption. Increasing the compressive strength has a more positive impact than increasing the slab thickness.

0.45OPS mix with a compressive strength of 28.4 MPa has higher service and impact energy than 0.50OPS of compressive strength of 27.5 MPa and 0.60OPS of compressive strength of 26.0 MPa. 0.45OPS-MD slab 40 mm thick has the highest service and ultimate impact energy value of 98.10 J and 502.76 J, about 2.0 times and 8.2 times, respectively, higher than its control. Then, the 0.50OPS-MD slab 40 mm thick has the service and ultimate impact energy value of 61.31 J and 380.14 J, about 2.5 times and 10.3 times, respectively, higher than its control. Lastly, 0.60OPS-MD slab 40 mm thick has the service and ultimate impact energy value of 49.05 J and 318.83 J, about 4.0 times and 13.0 times, respectively, higher than its control.

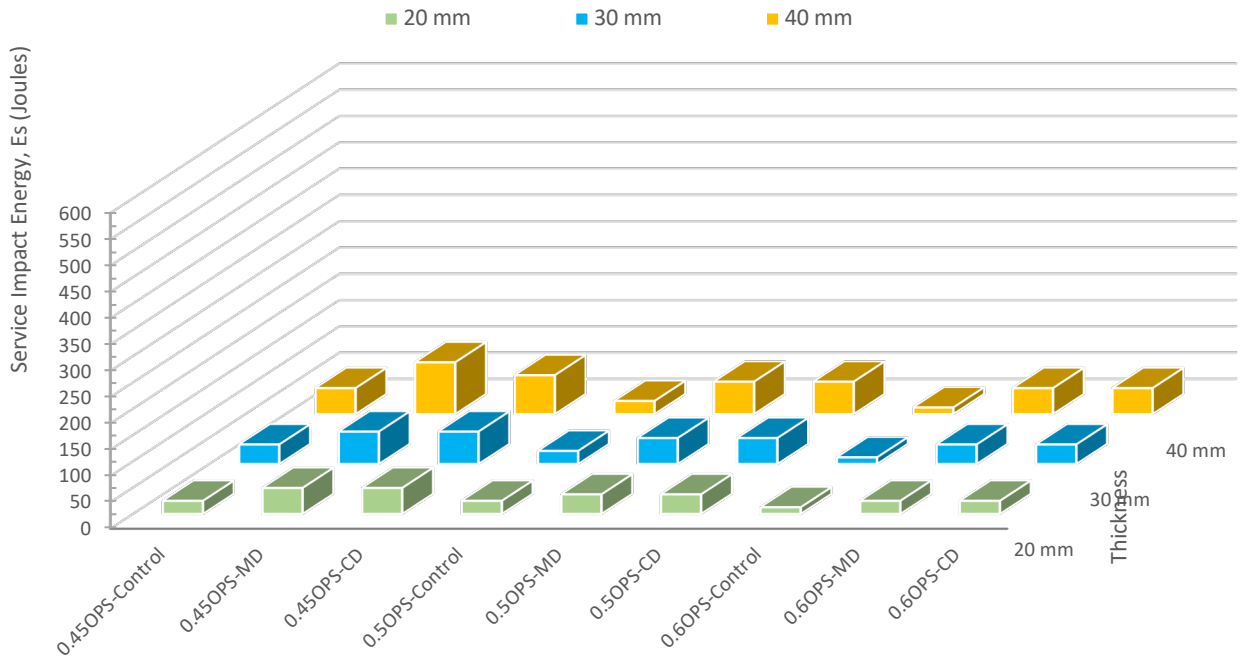

a) Service Impact Energy

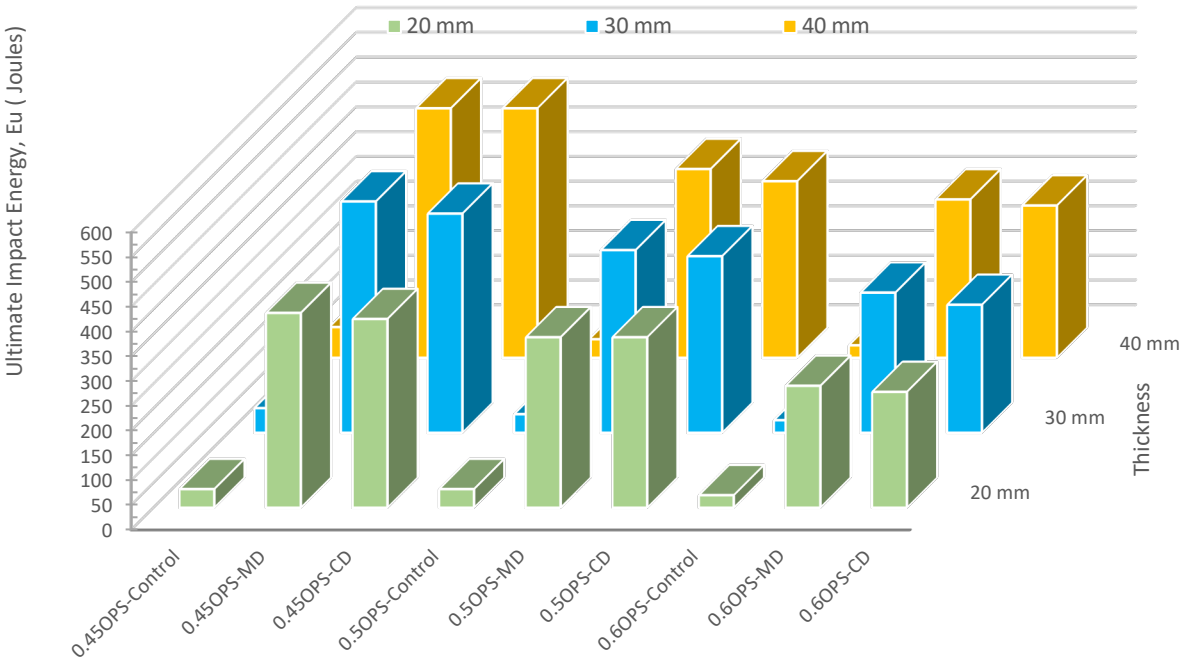

(a) Ultimate Impact Energy

Fig. 8: 3D Histogram Plot of Service and Ultimate Impact Energy against Thickness

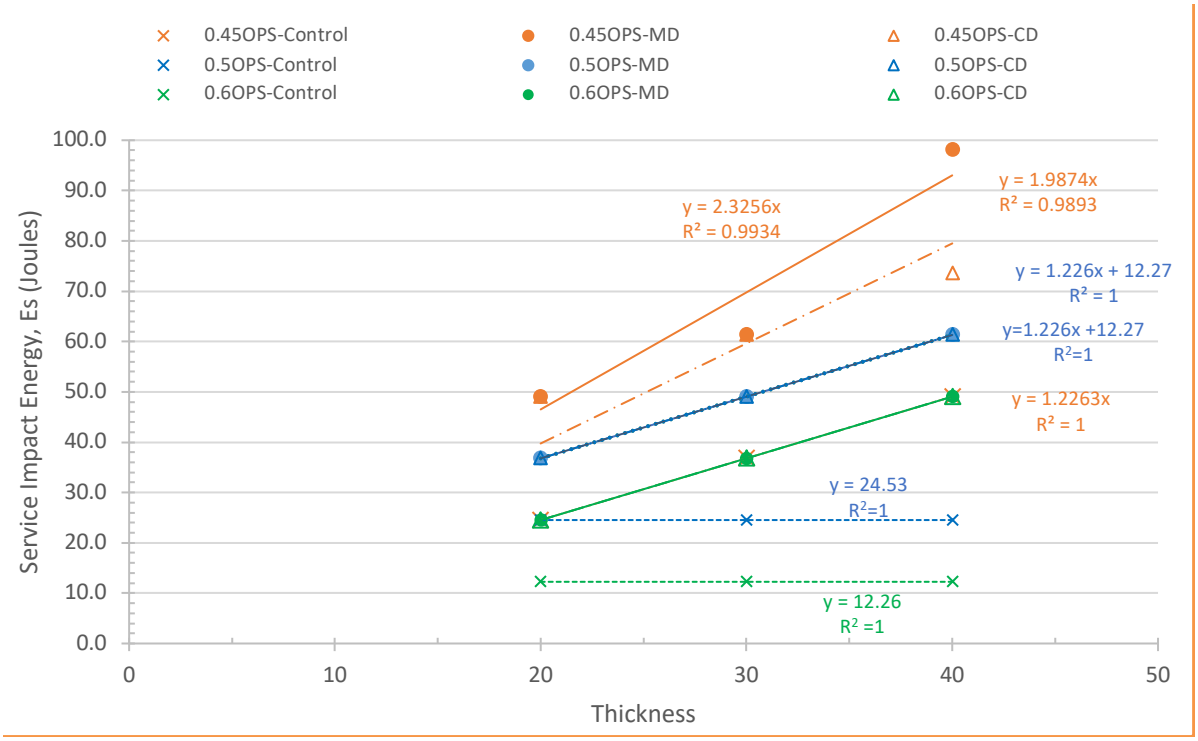

a) Service Impact Energy

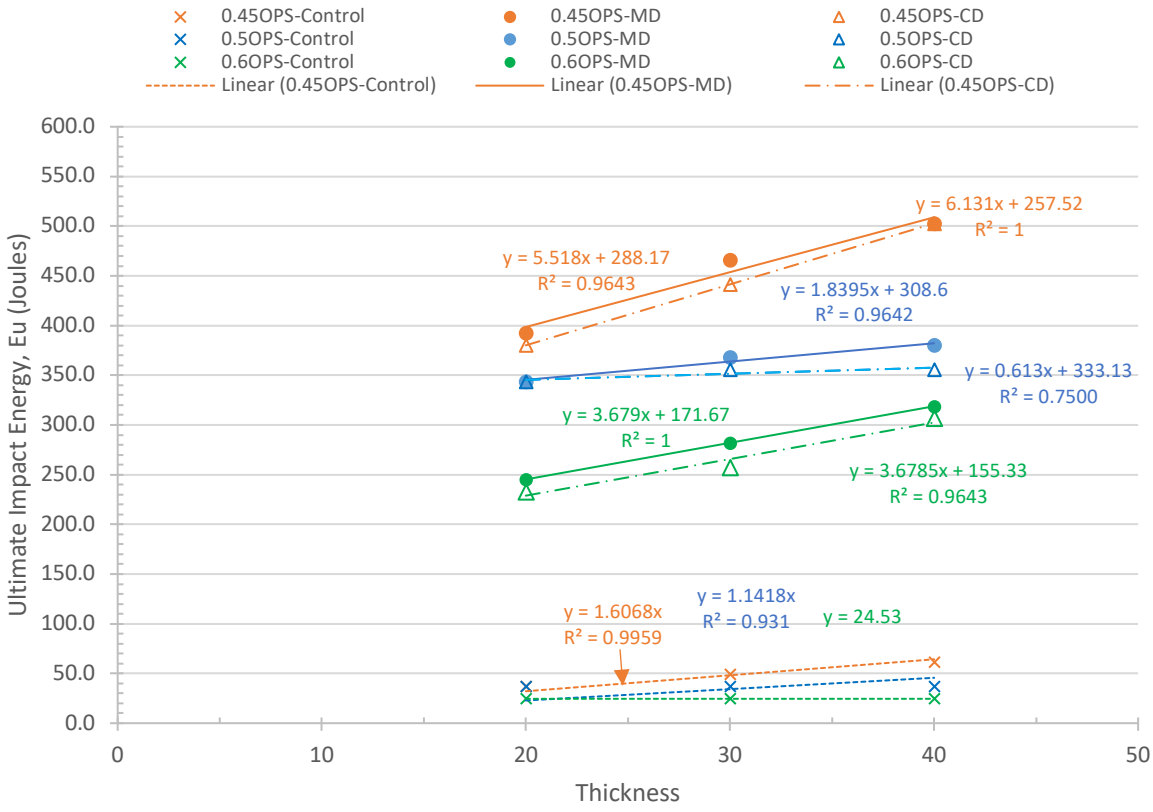

(b) Ultimate Impact Energy

Fig. 9: Relationship between (a) Service Impact Energy and (b)Ultimate Impact Energy against Thickness

Figure 9 shows the relationship between service and ultimate impact energy against thickness for different OPS variants and slab thickness.

The linear correlation for service impact energy (Es) against the volume fraction of PP fibre are as follows;

i) 0.45OPS

Control:

$Es_{(0.45OPS\text{-}Control)} = 1.2263t$ with $R^2 = 1$ (9)

Geogrid Main Direction (MD):

$Es_{(0.45OPS\text{-}MD)} = 2.3256t$ with $R^2 = 0.9934$ (10)

Geogrid Cross Direction (CD):

$Es_{(0.45OPS\text{-}CD)} = 1.9874t$ with $R^2 = 0.9893$ (11)

ii) 0.50OPS

Control:

$t \leq 20$ $Es_{(0.50OPS\text{-}Control)} = 1.2265t$

$t > 20$ $Es_{(0.50OPS\text{-}Control)} = 24.53$ with $R^2=1$ (12)

Geogrid MD & Geogrid CD:

$t \leq 20$ $Es_{(0.50OPS\text{-}MD)} = Es_{(0.50OPS\text{-}MD)} = 1.840t$

$t > 20$ $Es_{(0.50OPS\text{-}MD)} = Es_{(0.50OPS\text{-}MD)} = 1.226t + 12.27$ with $R^2=1$ (13)

iii) 0.60OPS

Control:

$t \leq 20$ $Es_{(0.60OPS\text{-}Control)} = 0.613t$

$t > 20$ $Es_{(0.60OPS\text{-}Control)} = 24.53$ with $R^2=1$ (14)

Geogrid MD & Geogrid CD:

$Es_{(0.60OPS\text{-}MD)} = Es_{(0.60OPS\text{-}MD)} = 1.2263t$

with $R^2=1$ (15)

The linear correlation for ultimate impact energy (Es) against the volume fraction of PP fibre are as follows;

i) 0.45OPS

Control:

$Es_{(0.45OPS\text{-}Control)} = 1.6068t$ with $R^2 = 0.995$ (16)

Geogrid MD:

$t \leq 20$ $Es_{(0.45OPS\text{-}MD)} = 19.927t$

$t > 20$ $Es_{(0.45OPS\text{-}MD)} = 5.518t + 288.17$

with $R^2 = 0.9643$ (17)

Geogrid CD:

$t \leq 20$ $Es_{(0.45OPS\text{-}CD)} = 19.007t$

$t > 20$ $Es_{(0.45OPS\text{-}CD)} = 6.1316t + 257.52$

with $R^2 = 1$ (18)

ii) 0.50OPS

Control:

$Es_{(0.50OPS\text{-}Control)} = 1.1418t$ with $R^2=0.931$ (19)

Geogrid MD:

$t \leq 20$ $Es_{(0.50OPS\text{-}MD)} = 17.270t$

$t > 20$ $Es_{(0.50OPS\text{-}MD)} = 1.8395t + 308.6$

with $R^2 = 0.9642$ (20)

Geogrid CD:

$t \leq 20$ $Es_{(0.50OPS\text{-}CD)} = 16.7178t$

$t > 20$ $Es_{(0.50OPS\text{-}CD)} = 0.613t + 333.13$

with $R^2 = 0.75$ (21)

iii) 0.60OPS

Control:

$t \leq 20$ $Es_{(0.60OPS\text{-}Control)} = 1.2265t$

$t > 20$ $Es_{(0.60OPS\text{-}Control)} = 24.53$

with $R^2=1$ (22)

Geogrid MD:

$t \leq 20$ $Es_{(0.60OPS\text{-}MD)} = 12.263t$

$t > 20$ $Es_{(0.60OPS\text{-}MD)} = 3.679t = 171.67$

with $R^2 = 1$ (23)

Geogrid CD:

$t \leq 20$ $Es_{(0.60OPS\text{-}CD)} = 1.1.445t$

$t > 20$ $Es_{(0.60OPS\text{-}CD)} = 3.6785t + 155.33$

with $R^2 = 0.9643$ (24)

The service and ultimate impact energy increases linearly as the thickness increases. An excellent linear and bi-linear correlation exists between the service and ultimate impact energy against the thickness, with R^2 values ranging from 0.7500 to 1.

4.3. Crack Resistance

Figure 10 shows the 3-D histogram plot between the service and ultimate crack resistance against the percentage of fibre VF for different support boundary conditions.

The service and ultimate crack resistance of slab specimens increased with increased of thickness and decrease with the increase in the OPS content. The geogrid in main direction performs slightly better than in the cross direction. The results indicate that slabs with 0.45OPS-MD with 40mm have the highest service and ultimate crack resistance value 98.10 N/mm^2 and 500.00 N/mm^2 about 2.00 and 13.81 times respectively higher than its control. The OPS variants with geogrid in the main direction have a slightly higher service and ultimate crack resistance of 1.00 -1.33 times and 1.01 - 1.02 times respectively than its control in the cross direction.

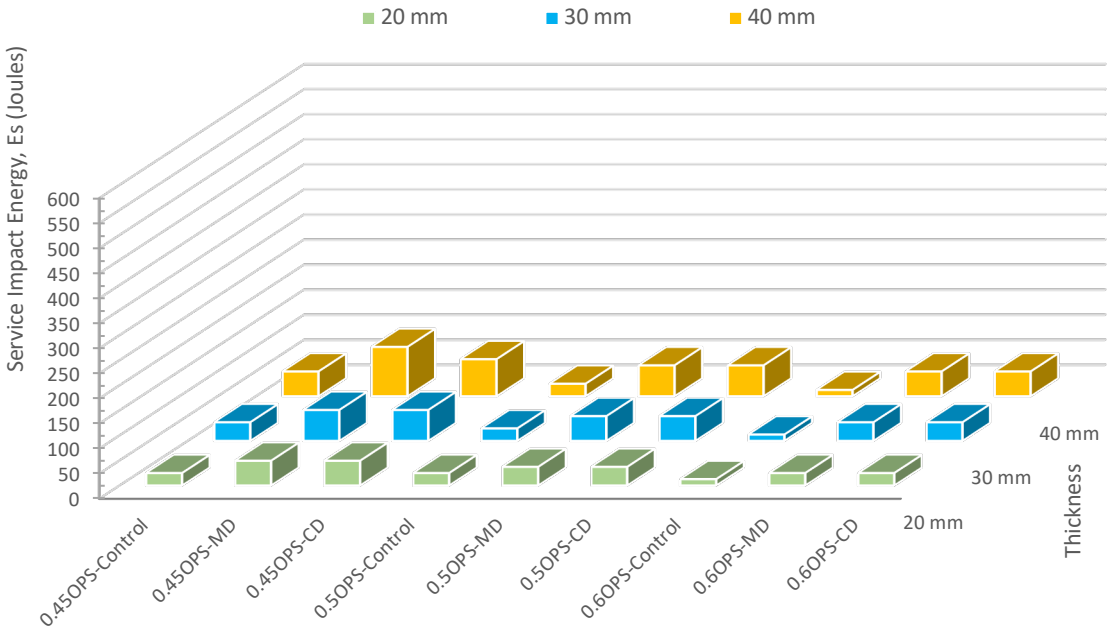

(a) Service Crack Resistance

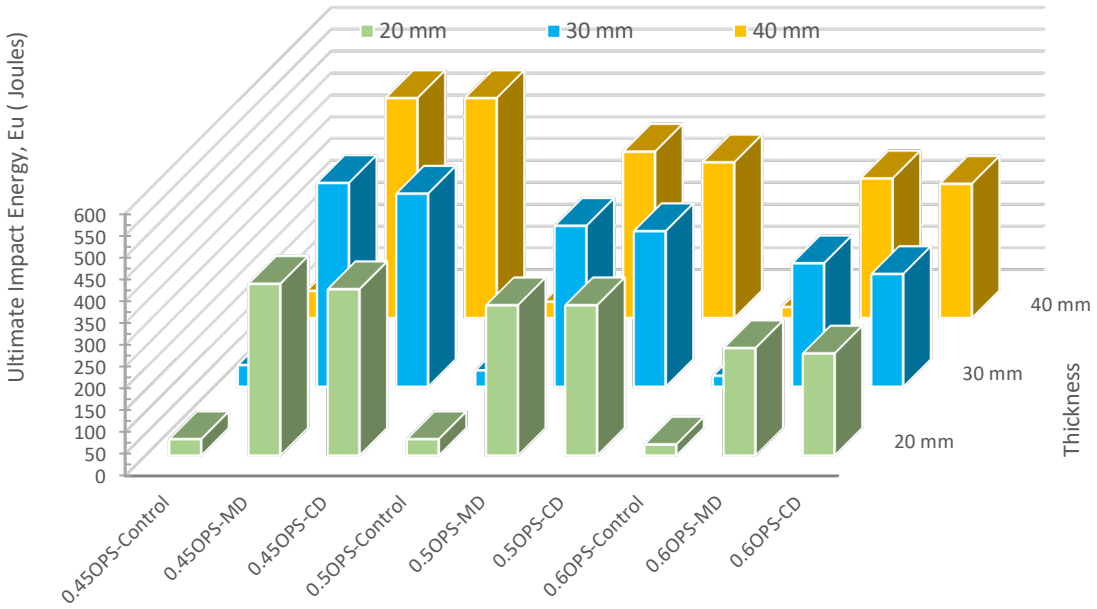

(b) Ultimate Crack Resistance

Fig. 10: Histogram Plot of Service and Ultimate Crack Resistance against Thickness

Figure 11 shows an excellent linear correlation between service crack resistance (Rs) and ultimate crack resistance (Ru) against thickness for the control, OPS content, and geogrid MD and CD orientation, with R^2 values ranging from 0.989 to 0.9995.

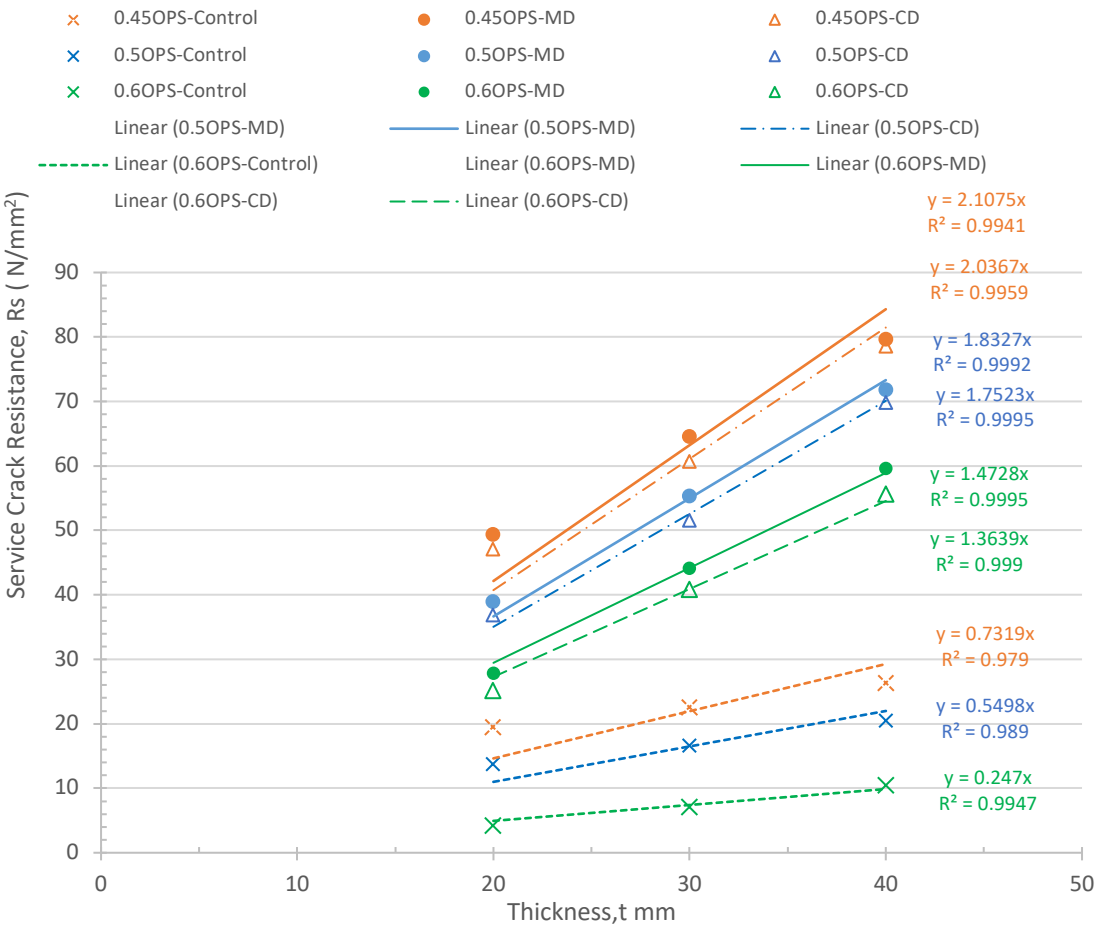

(a) Service Crack Resistance

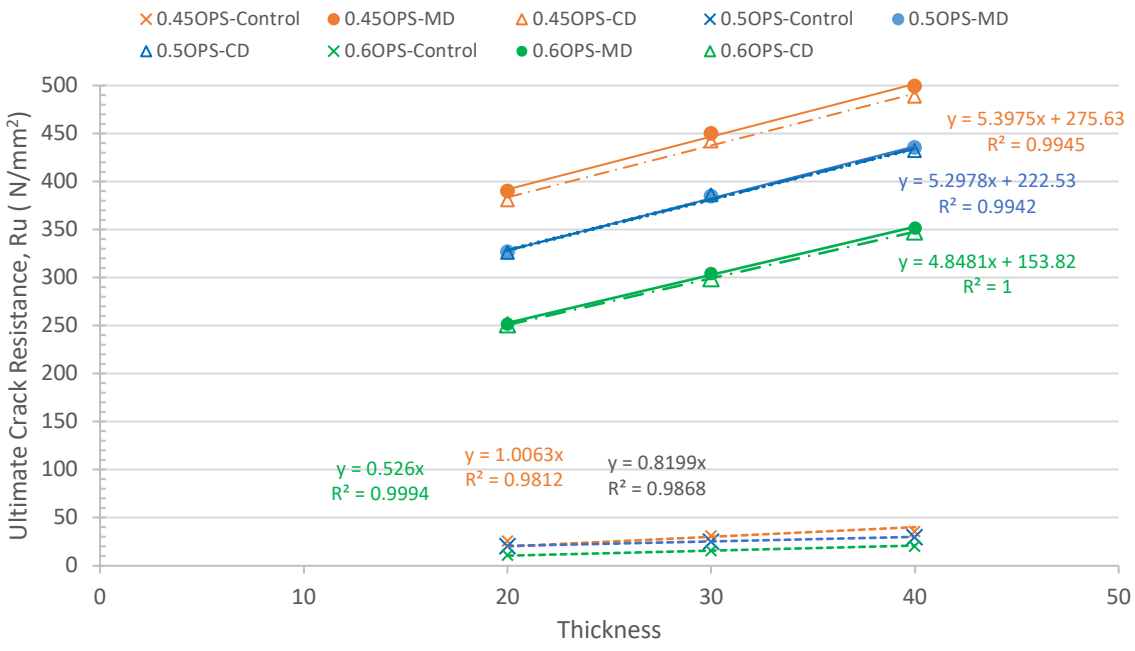

(b) Ultimate Crack Resistance

Fig. 11: Relationship between Service and Ultimate Crack Resistance against Thickness

The linear equations for service crack resistance (R_s) against slab thickness, as given in Figure 11 (a), are as follows:

i) 0.45OPS

Control:

$R_{s\,(0.45OPS)} = 0.7319t$ with $R^2 = 0.979$ (25)

Geogrid MD:

$R_{s\,(0.45OPS\text{-}MD)} = 2.1075t$ with $R^2 = 0.9941$ (26)

Geogrid CD:

$R_{s\,(0.45OPS\text{-}CD)} = 2.0367t$ with $R^2 = 0.9959$ (27)

ii) 0.50OPS

Control:

$R_{s\,(0.5OPS)} = 0.5498t$ with $R^2 = 0.9890$ (28)

Geogrid MD:

$R_{s\,(0.5OPS\text{-}MD)} = 1.8327t$ with $R^2 = 0.9995$ (29)

Geogrid CD:

$R_{s\,(0.5OPS\text{-}CD)} = 1.7523t$ with $R^2 = 0.9992$ (30)

iii) 0.6OPS

Control:

$R_{s\,(0.6OPS)} = 0.247t$ with $R^2 = 0.9947$ (31)

Geogrid MD:

$R_{s\,(0.6OPS\text{-}MD)} = 1.4728t$ with $R^2 = 0.9995$ (32)

Geogrid CD:

$R_{s\,(0.6OPS\text{-}CD)} = 1.3639t$ with $R^2 = 0.9990$ (33)

The equations for linear and bi-linear relationships of the OPS variants for the control and geogrid for ultimate crack resistance (R_u) against the slab thickness, as given in Figure 11 (b), are as follows;

i) 0.45OPS

Control:

$R_{u\,(0.45OPS)} = 1.0063t$ with $R^2 = 0.9812$ (34)

Geogrid MD:

(t <20 mm) $R_{u\,(0.45OPS\text{-}MD)} = 19.5918t$

(t ≥20 mm) $R_{u\,(0.45OPS\text{-}MD)} = 5.4938t + 281.96$

with $R^2 = 0.9971$ (35)

Geogrid CD:

(t <20 mm) $R_{u\,(0.45OPS\text{-}CD)} = 19.179t$

(t ≥20 mm) $R_{u\,(0.45OPS\text{-}CD)} = 5.3975t + 275.63$

with $R^2 = 0.9945$ (36)

ii) 0.5OPS

Control:

$R_{u\,(0.5OPS)} = 1.0063t$ with $R^2 = 0.9812$ (37)

Geogrid MD:

(t <20 mm) $R_{u\,(0.5OPS\text{-}MD)} = 19.5918t$

(t ≥20 mm) $R_{u\,(0.5OPS\text{-}MD)} = 5.4938t + 281.96$

with $R^2 = 0.9971$ (38)

Geogrid CD:

(t <20 mm) $R_{u\,(0.5OPS\text{-}CD)} = 19.179t$

(t ≥20 mm) $R_{u\,(0.5OPS\text{-}CD)} = 5.3975t + 275.63$

with $R^2 = 0.9945$ (39)

iii) 0.6OPS

Control:

$R_{u\,(0.6OPS)} = 1.0063t$ with $R^2 = 0.9812$ (40)

Geogrid MD:

(t <20 mm) $R_{u\,(0.6OPS\text{-}MD)} = 19.5918t$

(t ≥20 mm) $R_{u\,(0.6OPS\text{-}MD)} = 5.4938t + 281.96$

with $R^2 = 0.9971$ (41)

Geogrid CD:

(t <20 mm) $R_{u\,(0.6OPS\text{-}CD)} = 19.179t$

(t ≥20 mm) $R_{u\,(0.6OPS\text{-}CD)} = 5.3975t + 275.63$

with $R^2 = 0.9945$ (42)

The service and ultimate crack resistance increase linearly as the thickness increases. An excellent linear and bi-linear correlation exists between the service and ultimate crack resistance against the thickness, with R^2 values ranging from 0.979 to 1.

4.4. Crack Resistance Ratio

Figure 12 shows the crack resistance ratio (Cr) against the thickness for each OPS variant for the control and geogrid reinforcement orientation.

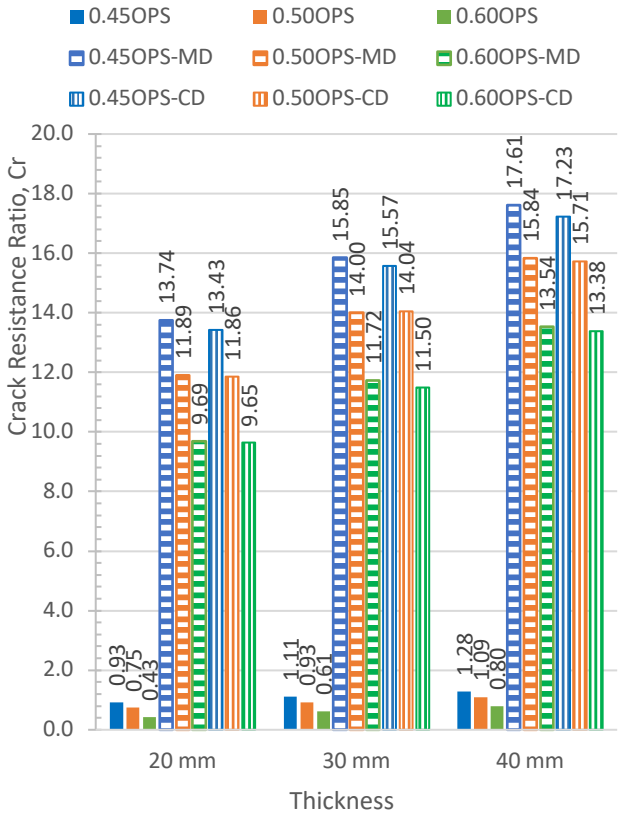

Fig. 12: Crack Resistance Ratio, C_r for OPS Variant of Different OPS Contents and Thickness

The crack resistance ratio, Cr, measures the effectiveness of the ultimate crack resistance performance against its compressive strength. The Cr is more effective for the slab with geogrid than the control without geogrid. The lower OPS content or a higher compressive strength has a better Cr ratio than the higher OPS content or lower compressive strength. The thicker slab has a higher Cr value than the thinner one. Among the various scenarios, the crack resistance ratio (Cr) is the highest for the 40mm slab with 0.45OPS-MD, registering a value of 17.61. This is followed by 0.45OPS-CD (17.23), 0.50OPS-MD (15.84), 0.50OPS-CD (15.71), 0.60OPS-MD (13.54), and finally 0.60OPS-CD (13.38). The Cr value for geogrid reinforcement in the main direction is better than in the cross direction.

Figure 13 shows an excellent bi-linear correlation between the service Cr and ultimate Cr for different OPS contents and thicknesses, with an R^2 value ranging from 0.9807 - 0.9994. The equations of the linear and bi-linear relationship of crack resistance ratio (Cr) for the OPS variants for the control and geogrid against the thickness are as follows;

i) 0.45OPS

Control:

$$Cr_{(0.45OPS)} = 0.0354t \text{ with } R^2 = 0.9807 \quad (43)$$

Geogrid MD:

(t <20 mm) $Cr_{(0.45OPS\text{-}MD)} = 0.6899t$

(t ≥20 mm) $Cr_{(0.45OPS\text{-}MD)} = 0.1935t + 9.9282$

$$\text{with } R^2 = 0.9971 \quad (44)$$

Geogrid CD:

(t <20 mm) $Cr_{(0.45OPS\text{-}CD)} = 0.6754t$

(t ≥20 mm) $Cr_{(0.45OPS\text{-}CD)} = 0.1901t + 9.7055$

$$\text{with } R^2 = 0.9945 \quad (45)$$

ii) 0.50OPS

Control:

$$Cr_{(0.5OPS)} = 0.0298t \text{ with } R^2 = 0.9868 \quad (46)$$

Geogrid MD:

(t <20 mm) $Cr_{(0.5OPS\text{-}MD)} = 0.5973t$

(t ≥20 mm) $Cr_{(0.5OPS\text{-}MD)} = 0.1971t + 7.9977$

$$\text{with } R^2 = 0.9983 \quad (47)$$

Geogrid CD:

(t <20 mm) $Cr_{(0.5OPS\text{-}CD)} = 0.5970t$

(t ≥20 mm) $Cr_{(0.5OPS\text{-}CD)} = 0.1927t + 8.0918$

$$\text{with } R^2 = 0.9942 \quad (48)$$

iii) 0.6OPS

Control:

$$Cr_{(0.6OPS)} = 0.0202t \text{ with } R^2 = 0.9994 \quad (49)$$

Geogrid MD:

(t <20 mm) $Cr_{(0.6OPS\text{-}MD)} = 0.4954t$

(t ≥20 mm) $Cr_{(0.6OPS\text{-}MD)} = 0.1926t + 5.8725$

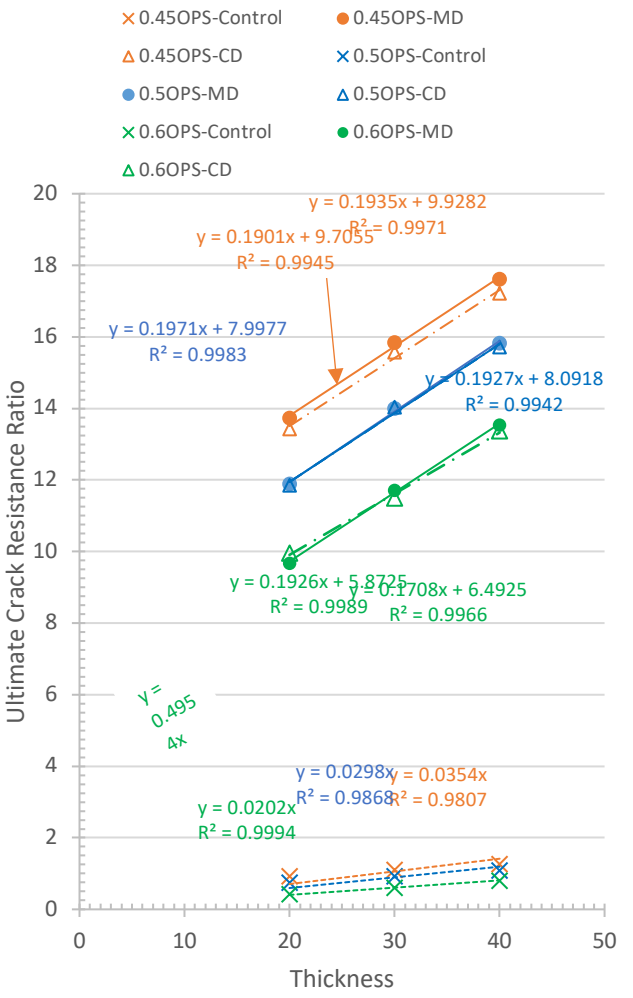

Fig. 13: Relationship between Crack Resistance Ratio, Cr against Thickness

$$\text{with } R^2 = 0.9989 \quad (50)$$

Geogrid CD:

(t <20 mm) $Cr_{(0.6OPS\text{-}CD)} = 0.4862t$

(t ≥20 mm) $Cr_{(0.6OPS\text{-}CD)} = 0.1708t + `6.4925$

$$\text{with } R^2 = 0.9966 \quad (51)$$

The geogrid in its main direction exhibits a slightly superior crack resistance ratio compared to its cross direction. Amongst the OPS variants with geogrid, the crack resistance ratio for OPS0.45 geogrid demonstrates superior performance followed by 0.50OPS than 0.60OPS geogrid with similar bi-linear trendlines against the slab thickness. The control and geogrid have a linear relationship and bi-linear relationship of crack resistance ratio (Cr), respectively, against the thickness.

4.5. Impact Residual Strength Ratio

Figure 14 shows the impact residual strength ratio against the thickness. The impact residual strength ratio helped to evaluate the post-crack behavior of the composites easily and could also be taken as a measure of the ductility imparted by the reinforcement incorporated into the slab. The residual strength ratio provides a valuable assessment of the post-crack behavior and serves as an indicator of the ductility of the geogrid reinforced slab.

The Irs values are higher for the slab with geogrid reinforcement than for the control. The higher the OPS content variant or a lower compressive strength has a better Irs ratio than the one with a lower OPS content or high compressive strength. Further thinner slab with geogrid reinforcement has a higher Irs value than the thicker one; as such, a thin slab with the geogrid has a better ductility performance. Among the various scenarios, the Irs is the highest for the 20mm slab with 0.60OPS-MD, registering a value of 10.0. This is followed by 0.60OPS-CD (9.5), 0.50OPS-MD (9.33), 0.50OPS-CD (9.33), 0.45OPS-MD (8.0), and finally 0.45OPS-CD (7.8). The post-cracking ductility for geogrid reinforcement in the main direction is better than in the cross direction.

Figure 15 shows an excellent linear relationship between OPS variants' impact residual ratio (Irs) against the slab thickness. The equations of the linear relationship of impact residual strength ratio against the thickness are as follows;

i) 0.45OPS

Control:

$$Irs_{(0.45OPS)} = -0.0125t + 1.735 \text{ with } R^2 = 0.9586 \quad (52)$$

Geogrid MD:

$$Irs_{(0.45OPS\text{-}MD)} = -0.0585t + 9.2317 \text{ with } R^2 = 0.9677 \quad (53)$$

Geogrid CD:

$$Irs_{(0.45OPS\text{-}CD)} = -0.131t + 10.623 \text{ with } R^2 = 0.8991 \quad (54)$$

ii) 0.50OPS

Control:

$$Irs_{(0.5OPS)} = 1.5 \text{ with } R^2 = 1 \quad (55)$$

Geogrid MD:

$$Irs_{(0.5OPS\text{-}MD)} = -0.1565t + 12.372 \text{ with } R^2 = 0.9905 \quad (56)$$

Geogrid CD:

$$Irs_{(0.5OPS\text{-}CD)} = -0.1765t + 12.755 \text{ with } R^2 = 0.9895 \quad (57)$$

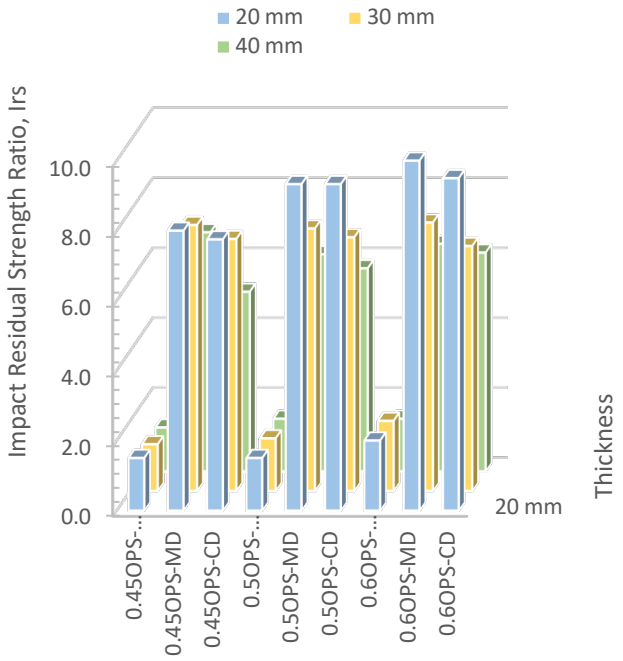

Fig. 14: Impact Residual Strength Ratio, Irs against Thickness

iii) 0.6OPS

Control:

$$Irs_{(0.6OPS)} = -0.025t + 2.5833 \text{ with } R^2 = 0.7500 \quad (58)$$

Geogrid MD:

$$Irs_{(0.6OPS\text{-}MD)} = -0.1725t + 13.307 \text{ with } R^2 = 0.9647 \quad (59)$$

Geogrid CD:

$$Irs_{(0.6OPS\text{-}CD)} = -0.1625t + 12.458 \text{ with } R^2 = 0.9119 \quad (60)$$

The geogrid in the main direction exhibits a superior impact residual strength ratio in its main direction as compared to its cross direction. Amongst the OPS variants with geogrid, the crack resistance ratio for OPS0.60 generally demonstrates superior performance followed by 0.50OPS than 0.45OPS with a linear trendline against the slab thickness. However, at a higher thickness of about 40mm, the 0.45OPS-MD with geogrid has a better impact residual strength ratio than the other OPS geogrid variants—the impact residual strength ratio decreases as the thickness increases. An excellent linear correlation exists between the impact residual strength ratios against the thickness, with R2 values ranging from 0.7500 to 1.

4.6 Failure Modes

The segmental failure modes of the control and geogrid mesh orientation for the service and ultimate crack resistance are shown in Table 3.

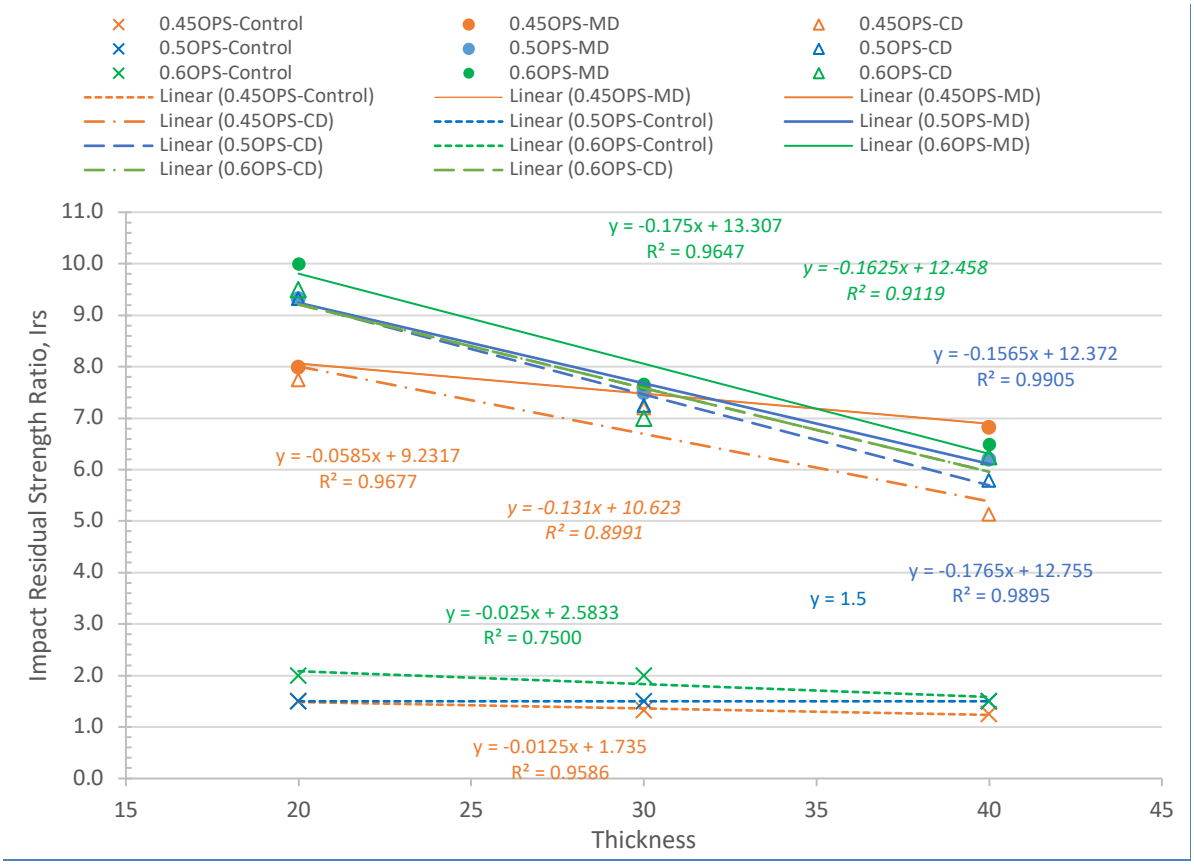

Fig. 15: Relationship between Impact Residual Strength Ratio, Irs against Thickness

Table 3: Failure Modes of a Typical Slab for the Control and Geogrid with Different Orientations at Service and Ultimate Impact Loads

No	Samples	Service Crack at Distal Face	Remarks	Ultimate Crack at Distal Face	Remarks
1	30 mm thick 0.45OPS (Control) 2-Support Condition	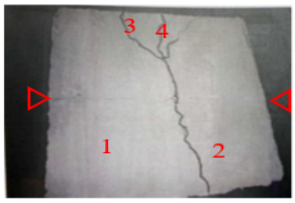	N(s) = 2 blows Crack at distal face with 2 main and 2 minor segmental crack zones	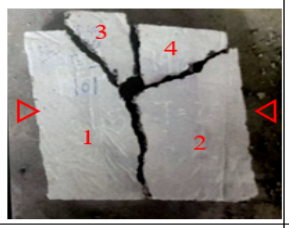	N(u) = 4 blows 2 major and 2 minor segmental failure zones were generated
2	30 mm thick 0.45OPS (Geogrid in Main Direction) 2-Support Condition	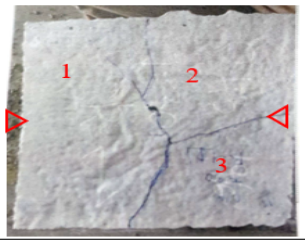	N(s) = 5 blows Cracks at distal face with 3 segmental zones	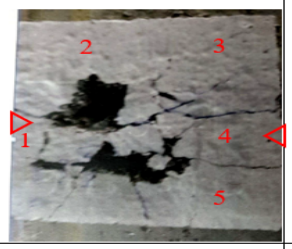	N(u) =38 blows 6 segmental failure zones were generated with larger perforation damage by local crushing and punching shear
3	30 mm thick 0.45OPS (Geogrid in Cross Direction) 2-Support Condition	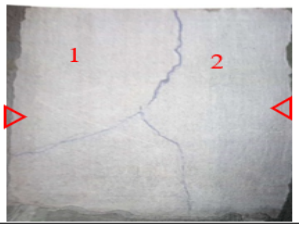	N(s) = 5 blows Cracks at distal face with 3 segmental zones	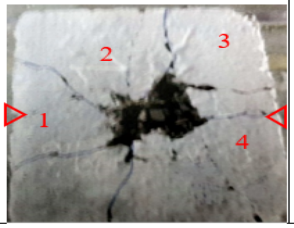	N(u) = 36 blows 6 segmental failure zones with smaller perforation damage by local crushing and punching shear

When an impact load is applied at the frontal face of concrete, it can develop tensile cracking and spalling on the distal face. This occurs because of the propagation of reflected tensile waves from the point of impact. The point of contact on the frontal face also experiences localized damage, likely resulting from compression failure that causes concrete crushing. Occasionally, overly reinforced concrete slabs can fail due to punching shear without exhibiting segmented failure zones. Typically, cracks initiate from the center and propagate toward the edge of the distal face under tensile stress.

Cracks started from the middle of the slab and progressively spread toward supports under service loads. However, a larger crack distribution with a larger damaged area was recorded under ultimate loads. It is observed that the geogrid in the main direction and cross direction mode of failure is similar, except the main direction one sustained a bigger perforation damage area due to local crushing and punching shear failure than the geogrid in the cross direction one at ultimate condition due to its effectiveness in sustaining a greater impact energy. The geogrid mesh effectively bridges the macro cracks, preventing the segments from collapsing completely at the ultimate point of failure.

Under service conditions, there are fewer segmental failure zones than in ultimate conditions. As the number of blows increases, the number of segmental failure zones also increases with perforation damage at the center area of the slab. The geogrid mesh prevents discrete concrete segment failures when the ultimate impact energy is applied to a slab specimen. This is achieved through its high ductility, allowing it to absorb the impact energy without causing a complete collapse.

5 Conclusions

This research evaluates the effect of the thickness and geogrid orientation on the impact behavior of lightweight OPS concrete under a low-velocity drop-weight impact test. The design mix consisted of 0.45OPS, 0.50OPS, and

0.60OPS variants with geogrid mesh in the main and cross directions. A total of 36 sample slabs were prepared. The relationship of impact resistance of lightweight OPS-reinforced concrete slab reinforced against the thickness and geogrid orientation has been established. The results with the proposed equations indicate that an increase in thickness of the slab and geogrid in the main direction increases the impact energy absorption, crack resistance, crack resistance ratio, and impact residual strength ratio significantly with better post-cracking ductility behavior. 0.45OPS variant with geogrid performs better than the other variants in all the above impact factors except impact residual strength ratio, the 0.60OPS variant performs better. The conclusions according to the objective are as given below;

1. The service and ultimate impact energy for OPS variants for the control and with geogrid from the highest to the lowest are as follows: 0.45OPS > 0.50OPS > 0.60OPS. There were good linear and bi-linear equations against the thickness as proposed, with a minimum R^2 value ranging from 0.75 to 1.0.
2. The service and ultimate crack resistance for OPS variants for the control and with geogrid from the highest to the lowest are as follows: 0.45OPS > 0.50OPS > 0.60OPS. There were excellent linear and bi-linear equations against the thickness as proposed, with a minimum R^2 value ranging from 0.979 to 1.0.
3. The crack resistance ratio for OPS variants for the control and with geogrid from the highest to the lowest are as follows: 0.45OPS > 0.50OPS > 0.60OPS. There were excellent linear and bi-linear equations as proposed against the thickness, with a minimum R^2 value ranging from 0.9807 to 1.0.
4. The impact residual strength ratio for OPS variants for the control and with geogrid from the highest to the lowest generally are as follows: 0.60OPS > 0.50OPS> 0.45OPS. There were good linear and bi-linear equations as proposed against the thickness with a minimum R^2 value ranging from 0.75 to 1.0.
5. The geogrid for all OPS variants exhibits a slightly superior impact behavior in its main direction compared to its cross direction.
6. Service cracks have fewer segmental zones of failures than ultimate cracks conditions for the geogrid. The geogrid in the main direction and cross direction mode of failure is similar, except the main direction one sustained a bigger perforation damage area due to local crushing and punching shear failure than the geogrid in the cross direction. The geogrid mesh effectively bridges the macro cracks, preventing the segments from collapsing completely at the ultimate point of failure.

Acknowledgments

The authors would like to thank the INTI International University, Malaysia for the financial support for the publication of this article.

References

[1] Abdul Rahman, N., Tan, A. S. H., Waqbitu, F. and Roslan, N. H. (2020), The effectiveness of oil palm shell (OPS) as major aggregate replacement in concrete, IOP Conf. Ser.: Earth. 476 (2020) 012-019. DOI 10.1088/1755-1315/476/1/012019.Brian, F. (2008), RCC-New developments and innovations, *Proceedings of the Brazilian International Roller Compacted Concrete (RCC) Symposium*, pp. 1–18, Salvador, Brazil, 2008.

[2] ACI Committee 544 (1996). State-of-the-art report on fibre-reinforced concrete. ACI Committee 544 report 544.1R-96. Detroit: American Concrete Institute;

1996.

[3] Alsayed, S. H., & Alsayed, M. A. (2019). Sustainable construction materials based on agricultural waste: A review. Journal of Cleaner Production, 240, 118146.

[4] Anandan, S., Jeyalakshmi, R., & Lakshmipathy, R. (2017). Agricultural waste fibres as sustainable construction materials: A review. Sustainable Materials and Technologies, 11, 1-19.

[5] Anil, Ö., Kantar, E. & Yilmaz, M. C. (2015). Low velocity impact behavior of RC slabs with different support types, Construction and Building Materials, 93 (2015) 1078-1088.

[6] Arunachalam, S., & Umarani, C. (2017). Use of palm kernel shell as lightweight aggregate in concrete: A review. Construction and Building Materials, 137, 271-280.

[7] Aslam, M., Shafigh, P., & Jumaat, M. Z. (2015). Structural lightweight aggregate concrete by incorporating solid wastes as coarse lightweight aggregate. Applied Mechanics and Materials, 747, 419-423.

[8] Aslam, M., Shafigh, P., Jumaat, M. Z. (2017). High strength lightweight aggregate concrete using blended coarse lightweight aggregate origin from palm oil industry. Sains Malaysia 46, 667-675. doi:10.17576/jsm-2017-4604-20.

[9] Beddoe, R., & Pearce, A. (2017). Agricultural waste ash: A potential reactive supplementary cementitious material. Cement and Concrete Composites, 77, 14-22.

[10] BS EN 12350-2:2009. Testing fresh concrete. Slump-test. BSI,2009.

[11] BS EN 12390-4:2009. Compressive strength of test specimens. BSI,2009.

[12] Che Muda, Z., Beddu, S., Alam, M.A., Malik, G., Birima, A. H., Thiruchelvam, S., Mustapha, K. N., Zaroog, O. S & Usman, F. (2015). The Effect of Different Boundary Support Condition and Reinforcement Orientation on Impact Resistance of Light Weight Oil palm shell Reinforced Geogrid Concrete Slab, Proc. of the Third Intl. Conf. on Advances in Civil and Structural Engineering - CSE 2015, pg 56-59, doi: 10.15224/ 978-1-63248-057-6-99.

[13] Cifuentes, H., García, F., Maeso, O., & Medina, F. (2013). Influence of the properties of polypropylene fibres on the fracture behavior of low-, normal-, and high-strength FRC. Construction and Building Materials, 45, 130-137.

[14] Farahani, J. N., Shafigh, P., Alsubari, B., Shahnazar, S., & Mahmud, H. B. (2017). Engineering properties of lightweight aggregate concrete containing binary and ternary blended cement. Journal of Cleaner Production, 156, 765-774.

[15] Ganesh, K., & Bhattacharyya, S. K. (2020). Utilization of agricultural waste materials as aggregates in concrete: A review. Journal of Cleaner Production, 278, 123988.

[16] Habeeb, G. A., Mahmood, S. H., & Ibrahim, M. H. (2016). Sustainable lightweight concrete using oil palm kernel shell. Construction and Building Materials, 121, 577-585

[17] Han, C.-G., Hwang, Y.-S., Yang, S.-H., & Gowripalan, N. (2005). Performance of spalling resistance of high-performance concrete with polypropylene fibre contents and lateral confinement. Cement and Concrete Research, 35, 1747–1753. http://dx.doi.org/10.1016/j.cemconres.2004.11.013.

[18] Kakooei, S., Akil, H. M., Jamshidi, M., & Rouhi, J. (2012). The effects of polypropylene fibres on the properties of reinforced concrete structures. Construction and Building Materials, 27, 73–77. http://dx.doi.org/10.1016/j.conbuildmat.2011.08.015.

[19] Kankam, C.K.(1999) Impact Resistance of palm kernel fibre-reinforced concrete pavement slab. Journal of Ferrocement 1999;29(4):279-86.

[20] Kareem, M. A., Raheem, A.A., Oriola, K. O., Abdulwahab,R. (2022), A review on application of oil palm shell as aggregate in concrete -Towards realising a pollution-free environment and sustainable concrete. Environmental Challenges, 8 (2022) 100531.

[21] Kumar, A., & Bhunia, D. (2021). Utilization of agricultural waste materials in sustainable construction: A comprehensive review. Journal of Cleaner Production, 281, 125349.

[22] Liew, Y. M., Mohd Nawi, M. N., Megat Johari, M. A., & Ramli, M. (2021). Impact Resistance and Flexural Properties of Lightweight Concrete Reinforced with Oil palm shell and Steel Fibres. Materials Today: Proceedings, 44, 4236-4242.

[23] Maghfouri, M., Shafigh, P., Aslam, M., 2018. Optimum oil palm shell content as coarse aggregate in concrete based on mechanical and durability properties. Adv. Mater. Sci. Eng. 4271497, 1–14. doi: 10.1155/2018/4271497

[24] Mahmoud, N. and Afroughsabet, V. (2010) Combined effect of silica fume and steel fibres on the impact resistance and mechanical properties of concrete. International Journal of Impact Engineering 37(2010) 879 – 886.

[25] Mannan, M.A., Alexandra, J., Ganapathy, C., Teo, D.C.L., 2006. Quality improvement of oil palm shell

(OPS) as coarse aggregate in lightweight concrete. Build. Environ. 41, 1239–1242.

[26] Md Akhir, M. F., Mohamed Sunar, N. A., & Jaafar, M. S. (2020). Impact Strength and Flexural Performance of Lightweight Oil palm shell Concrete Reinforced with Different Fibres. Journal of Advanced Research in Materials Science, 66(1), 16-25.

[27] Md Din, M. F., Megat Johari, M. A., Shahidan, S., Mohd Nawi, M. N., & Ali, A. A. A. (2017). Impact Resistance of Lightweight Concrete with Oil palm shell Aggregate. Key Engineering Materials, 742, 30-35.

[28] Mo, K.H., Yap, S. P., Alengaram, U. J., Jumaat, M. Z., Bu, C. H. (2014). Impact resistance of hybrid fibre-reinforced oil palm shell concrete. Construction and Building Materials, 50(2014)499–507.

[29] Mohd Nawi, M. N., Abdullah, N., Othman, N., & Shahidan, S. (2019). Impact Strength of Lightweight Concrete Reinforced with Oil Palm Shell. Journal of Engineering Science and Technology, 14(3), 1494-1506.

[30] Mukherjee, S., Rana, S., Sarkar, R., & Mitra, P. (2021). Utilization of agricultural waste for sustainable construction materials: A state-of-the-art review. Journal of Cleaner Production, 289, 125713.

[31] Nadeem, M., Noumowé, A., & Hjiaj, M. (2020). Valorization of agricultural and agro-industrial waste materials for the development of sustainable construction materials: A review. Journal of Cleaner Production, 246, 118960.

[32] Naik, T. R., Kraus, R. N., & Siddique, R. (2021). Valorization of agricultural and industrial waste in sustainable construction materials: A review. Journal of Cleaner Production, 282, 124346.

[33] Nuruddin, M. F., Arshad, M. F., & Hassan, M. K. (2011). Mechanical Properties and Impact Resistance of Lightweight Concrete Containing Oil palm shell (OPS) Aggregate. Construction and Building Materials, 25(3), 1228-1233.

[34] Okafor, F. O., & Zain, M. F. M. (2018). Utilization of oil palm shell as lightweight aggregate in concrete: A review. Construction and Building Materials, 185, 47-55.

[35] Rahmani, T., Kiani, B., Shekarchi, M., & Safari, A. (2012). Statistical and experimental analysis on the behavior of fibre reinforced concretes subjected to drop weight test. Construction and Building Materials, 37, 360–369. http://dx.doi.org/10.1016/j.conbuildmat.2012.07.068.

[36] Rajesh Kumar, K., Awoyera , P. O., Shyamala, G., Kumar, V., Gurumoorthy, N., Kayikci, S., Bendezu' Romero, L. M., Krishna Prakash, A. (2022), Structural Performance of Biaxial Geogrid Reinforced Concrete Slab, International Journal of Civil Engineering, (2022) 20:349–359 https://doi.org/10.1007/s40999-021-00668-y

[37] Ramakrishna, G. and Sundararajan, T. (2005) Impact strength of a few natural fibre reinforced cement mortar slabs: a comparative study, Cem. Concr. Compos. 27 (2005) 547–553. http://dx.doi.org/10.1016/j.cemconcomp.2004.09.006.

[38] Raut, S. P., & Ghosh, P. C. (2020). Use of agricultural and industrial waste in construction materials: A review. Construction and Building Materials, 248, 118614.

[39] Sharifi, Y., Jafari, R., & Roshan, G. (2021). Sustainable concrete production by incorporating agricultural waste materials: A review. Journal of Building Engineering, 42, 103321.

[40] Song, P. S., Hwang, S., & Sheu, B. C. (2005). Strength properties of nylon- and polypropylene-fibre-reinforced concretes. Cement and Concrete Research, 35, 1546–1550.

[41] Tahir, M. F. M., Saleh, M. A. M., Ibrahim, N. M., & Abd Rahman, N. A. (2019). Impact Resistance and Mechanical Properties of Lightweight Oil palm shell Concrete with Polypropylene Fibres. Construction and Building Materials, 224, 117-126.

[42] Vijay, T. J., Kumar, K. R., Vandhiyan, R., Mahender, K., Tharani, K. (2020) Performance of Geogrid Reinforced Concrete Slabs under Drop Weight Impact Loading IOP Conf. Series: Materials Science and Engineering, 981 (2020) 032070 IOP Publishing doi:10.1088/1757-899X/981/3/032070

[43] Yahaghi, J., Che Muda, Z. and Beddu, S. (2016), Impact resistance of oil palm shell concrete reinforced with polypropylene fibre, Construction and Building Materials, 123 (2016) 394–403.

[44] Yew, M. C., Gan, B. H., Lim, Y. M., & Lee, S. K. (2018). Flexural and Impact Performance of Reinforced Lightweight Oil palm shell Concrete. Journal of Advanced Concrete Technology, 16(7), 323-335.

[45] Han, B., Xie, H., Yang, S., & Liu, T. (2018). Performance of geogrid-reinforced concrete slabs under impact loads. Construction and Building Materials, 182, 254-262.

[46] Kheyroddin, A., & Bocciarelli, M. (2019). Experimental investigation of geogrid reinforced concrete slabs under impact loadings. Construction and Building Materials, 228, 116815.

[47] Mansouri, I., Pourdehnad, H., & Razzaghi, M. S. (2017). Experimental study on the behavior of

reinforced concrete slabs subjected to impact loads. Construction and Building Materials, 151, 713-724.

[48] Niu, Y., Xu, Z., Chen, W., & Liu, X. (2020). Experimental investigation on the impact response of geogrid-reinforced concrete slabs. Construction and Building Materials, 251, 118940.

[49] Shi, H., Tan, Y., & Li, G. (2021). Experimental investigation on the impact behavior of geogrid-reinforced concrete slabs. Construction and Building Materials, 281, 122505.

[50] Wang, Y., Chen, Z., & Zhu, H. (2019). Experimental study on the impact resistance of geogrid-reinforced concrete slabs. Construction and Building Materials, 211, 848-857.

Biography:

Zakaria Che Muda earned his Ph. D. degree in Built Environment from University of Malaya. He is currently a Professor at the Department of Civil Engineering, INTI International University. He has published over 100 papers in international journals. His research interests are focused on fibre reinforced concrete, lightweight concrete and impact resistance structures.

Mohamed Ahmed Hafez earned his Ph. D. degree in Civil Engineering From University of Malaya. He is currently an Associate Professor at the Department of Civil Engineering, INTI International University. He has published over 55 papers in international journals. His research interests are focused on Dam risk assessment, slope stability and soft ground improvement.

Md Ashraful Alam: earned his Ph. D. in Structural Engineering from University of Malaya in 2010. He is currently a Professor at Department of Civil Engineering, University of Asia Pacific, Bangladesh. He has published about 71 papers in international conference proceedings and journals. His research interests include retrofitting of structures and natural fibre laminates for structural strengthening.

Ghazal Malik is currently working as Coastal Engineering at Surbana Jurong Group Singapore. She get her M.Sc Civil Engineering in 2013 from Nanyang Technological University Singapore and her B.Eng Civil Engineering in 2012 from University Tanaga Nasional.

As'ad Zakaria is currently a Ph. D student at the Institute of Energy Systems, School of Engineering, University of Edinburgh, Edinburgh, UK. He has published more than 10 papers in international journals. His research interest is in monte carlo simulation, electric vehicle, power system analysis and renewable energy system.

Appendix 1: Results of the Experimental Impact Test

OPS Variant	Thickness (mm)	Crack Condition	N[1]	E[2] (Joule)	R[3] (N/mm^2)	fcu[4] (N/mm^2)	Cr[5]	Irs[6]
0.45OPS Control	20	Service	2	24.53	19.56	28.4		
		Ultimate	3	36.79	26.32	28.4	0.93	1.50
	30	Service	3	36.79	22.58	28.4		
		Ultimate	4	49.05	31.45	28.4	1.11	1.33
	40	Service	4	49.05	26.34	28.4		
		Ultimate	5	61.31	36.21	28.4	1.28	1.25
0.45OPS-MD	20	Service	4	49.05	49.45	28.4		
		Ultimate	32	392.40	390.13	28.4	13.74	8.00
	30	Service	5	61.31	64.58	28.4		
		Ultimate	38	465.98	450.20	28.4	15.85	7.60
	40	Service	6	73.58	78.56	28.4		
		Ultimate	41	502.76	500.00	28.4	17.61	6.83
0.45OPS-CD	20	Service	4	49.05	47.10	28.4		
		Ultimate	31	380.14	381.26	28.4	13.43	7.75
	30	Service	5	61.31	60.74	28.4		
		Ultimate	36	441.45	442.18	28.4	15.57	7.20
	40	Service	8	98.10	79.63	28.4		
		Ultimate	41	502.76	489.21	28.4	17.23	5.13
0.5OPS Control	20	Service	2	24.53	13.75	27.5		
		Ultimate	3	36.79	20.57	27.5	0.75	1.50
	30	Service	2	24.53	16.60	27.5		
		Ultimate	3	36.79	25.53	27.5	0.92	1.50
	40	Service	2	24.53	20.53	27.5		
		Ultimate	3	36.79	30.01	27.5	1.09	1.50
0.5OPS-MD	20	Service	3	36.79	38.99	27.5		
		Ultimate	28	343.35	327.06	27.5	11.89	9.33
	30	Service	4	49.05	55.35	27.5		
		Ultimate	30	367.88	385.10	27.5	14.00	7.50
	40	Service	5	61.31	71.87	27.5		
		Ultimate	31	380.14	435.5	27.5	15.84	6.20
0.5OPS-CD	20	Service	3	36.79	36.93	27.5		
		Ultimate	28	343.35	326.16	27.5	11.86	9.33
	30	Service	4	49.05	51.60	27.5		
		Ultimate	29	355.61	386.12	27.5	14.04	7.25
	40	Service	5	61.31	69.88	27.5		
		Ultimate	29	355.61	432.11	27.5	15.71	5.80
0.6OPS Control	20	Service	1	12.26	4.25	26.0		
		Ultimate	2	24.53	11.11	26.0	0.43	2.00
	30	Service	1	12.26	7.08	26.0		
		Ultimate	2	24.53	15.88	26.0	0.61	2.00
	40	Service	2	24.53	10.48	26.0		
		Ultimate	3	36.79	20.68	26.0	0.80	1.50
0.6OPS-MD	20	Service	2	24.53	27.90	26.0		
		Ultimate	20	245.25	251.87	26.0	9.69	10.00
	30	Service	3	36.79	44.14	26.0		
		Ultimate	23	282.04	304.76	26.0	11.72	7.67
	40	Service	4	49.05	59.72	26.0		
		Ultimate	26	318.83	351.99	26.0	13.54	6.50
0.6OPS-CD	20	Service	2	24.53	25.20	26.0		
		Ultimate	19	232.99	250.91	26.0	9.65	9.50
	30	Service	3	36.79	40.83	26.0		
		Ultimate	21	257.51	299.01	26.0	11.50	7.00
	40	Service	4	49.05	55.66	26.0		
		Ultimate	25	312.50	347.87	26.0	13.38	6.37